Development of Electrical Impedance Imaging System for Continuous Monitoring of Lung Diseases

Aniqa Tabassum
Department of Electrical and Electronic Engineering
University of Dhaka
Dhaka, Bangladesh
aniqatab@gmail.com

Md. Adnan Kiber
Department of Electrical and Electronic Engineering
University of Dhaka
Dhaka, Bangladesh
md.adnan.kiber@gmail.com

Abstract—**This paper presents a new protocol and measurement technique of Electrical Impedance Imaging for continuous monitoring of lung diseases. In this proposed system, there are eight voltage measurement electrodes placed on the patient's back, along the outline of each lung, and two constant current injection electrodes, one posterior and one anterior. Traditional EIT based lung imaging methods used electrodes placed at a cross-sectional level on the chest with current injection and voltage measurement done in a cyclic order. Compared to such systems, the proposed model is found to be more sensitive and requires a new design of Hardware and Interface, including Constant Current Injector, Potential Measurement Unit, a microcontroller-based Switching System, and a data acquisition system. The system has less complexity and computational burden. The proposed system was tested on a Phantom Model resembling the human thorax, according to International Standards. Data was collected using a saline solution of conductivity 1.52 S/m, resembling average lung fluid conductivity. Robustness of the proposed approach in disease detection was investigated by testing the phantom with anomalies. The system can detect the presence of such anomalies representing diseased lung tissues. However, it needs further development and testing in clinical settings.**

***Contribution*—A new, more sensitive, and simple lung imaging system was developed.**

Keywords— Electrical impedance imaging, phantom model, impedance profile, electrode configuration, lung imaging.

I. INTRODUCTION

Electrical Impedance Tomography (EIT) is a technique where an image of the conductivity distribution within a part of the body is inferred from potentials measured through surface electrodes. EIT is safe, non-invasive, radiation-free and portable, and thus enables continuous real-time monitoring of lung function over extended periods. The principle of EIT involves the continuous measurement of potentials, resulting from the cyclic injection of low-amplitude and high-frequency alternating currents, through electrodes placed on the circumference of the subject of interest. EIT generates cross-sectional images of electrical impedance inside the human body. Its usefulness in medical imaging has been explored in numerous studies over time. The basic principle of EIT is over thirty years old, yet the growing number of publications in this field suggest possible clinical applications of this method in recent times. Due to the constantly improving quality of hardware and data processing modalities, EIT is being considered a promising technique in a large number of medical applications.

The theoretical concept of EIT was described almost over 30 years ago [1]. Earlier, hardware design, image reconstruction algorithm and software, and possible practical applications of EIT were introduced by Barber and Brown at the Department of Medical Physics and Clinical Engineering, Sheffield, UK. They named this technique Applied Potential Tomography, which is called Electrical Impedance Tomography (EIT) today, studied absolute and functional EIT images, and suggested its application in clinical practice. Extensive development of this method has taken place, since then, to apply EIT in a clinical environment [2]. EIT was first used in geology and archaeology to produce images of cavities and void spaces [3]. Henderson and Webster were the first to introduce images of the impedance of human tissues [4]. The main focus of EIT imaging applications, was to detect and locate pathologies, such as the presence of cancerous cells for breast [5],[6] and prostate [7] since malignant tissue has significantly different characteristics compared to benign tissue**.** One of the biggest advantages that EIT offers is the monitoring of lung function dynamics in ventilator aided ICU patients [8]. Inspiration leads to a rise in impedance value of tissues, proportionate to the volume of air inhaled, and can be monitored using EIT [9]. Detection of breathing rate and blood flow in the human body are some major monitoring applications of EIT [10]. In the case of mechanical ventilation, EIT may be able to potentially guide a patient-specific optimal level of support. For obstructive lung diseases, like COPD, emphysema, and asthma, lung function inhomogeneity cannot be observed by existing methods. EIT shows improved disease detection in this case [11],[12]. Neural and brain activity have also been imaged using EIT [13]. Applications also include the detection of pulmonary edema in the lungs, monitoring of gastric emptying, lung perfusion, and cardiac function.

The physical aspect of EIT lung imaging is built on the determination of impedance or conductivity distributions within the human thorax. Electrodes are fixed around a patient's chest. Alternating currents of high frequency and low amplitude are applied to the chest by successive electrode pairs and potential obtained from the remaining pairs [14]. Commercial systems mostly have 16 or 32 electrodes. The greater the number of electrodes, the better the resolution, but complexity and computational burden rises as a result. A full circle of all the electrodes produces a voltage profile, also called a frame, which is then used to reconstruct a tomographic image of the thorax. Sheffield Backprojection Algorithm was the basis of EIT image reconstruction initially, though several new algorithms with improved characteristics and faster implementation are being developed now [15]. The obtained image reflects the impedance distribution within the lungs. The major challenge, though, was extracting time-varying impedance information. The different data sampling techniques and analysis methods have divided EIT into the following categories [16]:

(1) functional EIT (f-EIT) [17]
(2) absolute EIT (a-EIT) [18], [19]
(3) EIT spectroscopy or multi-frequency EIT (MF-EIT)

To continuously monitor lung function, several studies have been carried out using either custom designed or commercially available EIT devices [20].

EIT is a non-hazardous and noninvasive monitoring technique [21]. Though the images have poor spatial resolution, the high temporal resolution makes it capable of monitoring impedance changes over time**.** Unlike conventional radiography or computed tomography (CT), EIT is free from radiation exposure and allows continuous observation of lung function over extended periods [22]. EIT measurement devices are comparatively inexpensive, and there have not been any such instances to expect harmful biological effects from the small amplitude currents applied in the process**.** However, EIT is better suited for monitoring dynamic changes in time in a particular patient, rather than comparisons between individuals. Another problem is the practicality of the placement of electrodes, specifically in bedridden patients and newborn children. EIT images show relatively poor spatial and contrast resolution and only allow observation of a slice of the lungs, and thus makes it difficult to obtain accurate morphological information.

The rest of this paper is organized as follows. In Section II, the system design has been introduced. Section III presents the different tests to evaluate system performance with their results, and Section IV includes the discussion. Finally, the paper is concluded in Section V.

II. SYSTEM DESIGN

The basic block diagram of the proposed system is given in this section, followed by the circuitry of the individual units.

From research simulation results, a new EIT method was proposed, which was found to be more sensitive than the existing methods [23], [24].

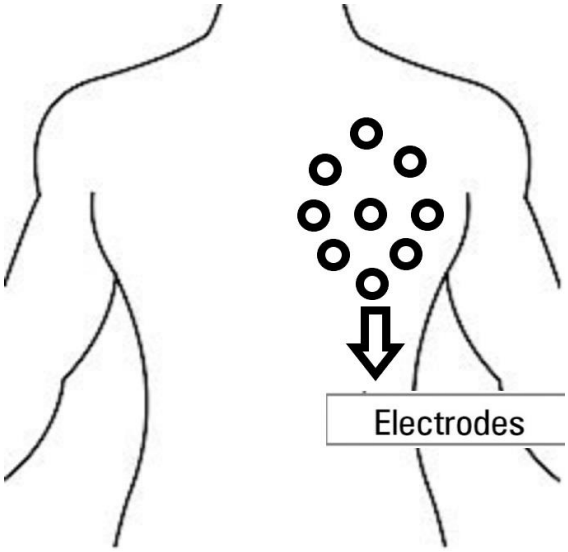

Figure 1. Proposed EIT method for Lung Disease Detection (Back view)

This new design, as shown in Fig. 1, includes 8 voltage measurement electrodes placed on the patient's back along the outline of each lung and two constant current injection electrodes, one posterior, and one anterior.

The block diagram in Fig. 2 illustrates the complete workflow of the system. The constant current source injects a current of frequency 50 kHz and amplitude 1 mA into the phantom model. The phantom solution conducts the current, and the developed voltages are obtained through surface electrode measurements. The voltages are multiplexed in a sequence set by the microcontroller and passed on to the potential measurement unit, where they are processed before sending it to the computer for analysis.

The proposed Electrical Impedance Imaging System has the following components:

A. Constant Current Injector

For ease of measurement and analysis, a constant current source is always desirable in biomedical applications. The

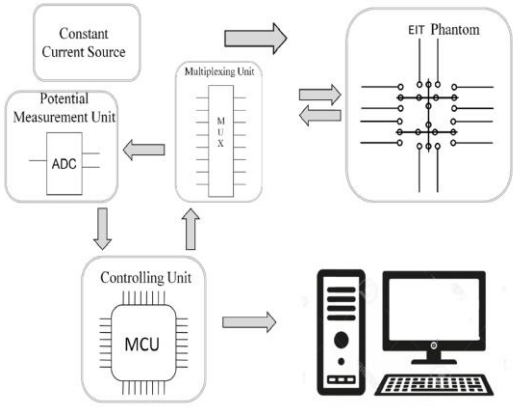

Figure 2. Block Diagram for proposed EIT system

design of the constant current injector is based on the modified Howland current pump, used for better output stability and simplicity of design. Fig. 3 shows the current injector circuit schematic diagram.

Components:

- Signal Generator (AD9851 DDS)
- Modified Howland Current Source

The injected current is of high frequency to avoid stimulation and tissue heating, and low amplitude to ensure the safety of the patient. The implemented current source characteristics are:

- Current Output : 1mA
- Signal Frequency : 50KHz
- Output Stability : ~4KΩ (Load)

B. Potential Measurement Unit

Bioimpedance ranges from around 10Ω ~ 100Ω (found from different experiments). Applying 1mA constant current to a biological subject would result in a voltage signal of 10mV~ 100mV, which is significantly small, and variation at this level may not be accurately measurable. Thus the signal needs to be amplified for correct signal acquisition. Also, the obtained signal is bipolar, which cannot be read directly using an ADC. So amplification needs to be set at such a level that the signal remains within the maximum measurement limit of the ADC even after adding a DC offset to shift the amplified signal completely above zero level.

The potential measurement unit block diagram is given in Fig. 4. The input high pass filter eliminates noise entering from the system and the surroundings. The cutoff frequency is set at 1.5 kHz less than 20% of the desired signal frequency, i.e., 50 kHz, according to the rule of thumb. AD624 is a high precision, low noise instrumentation amplifier with high gain accuracy and linearity, and is ideal for use in this system.

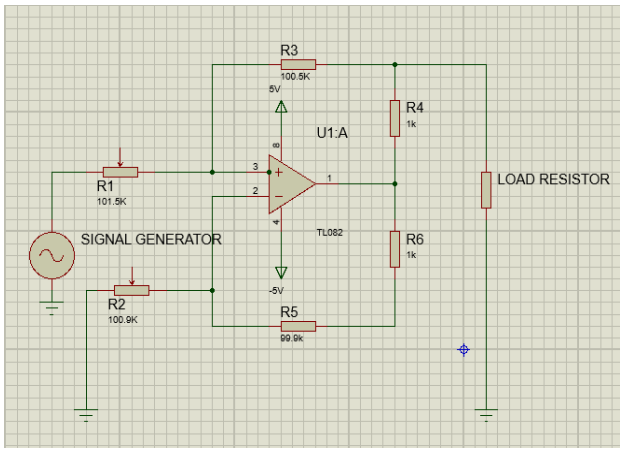

Figure 3. Current Injector Circuit

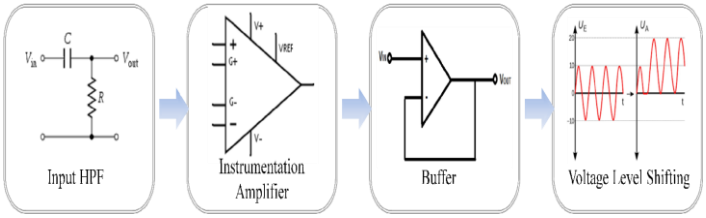

Figure 4. Potential Measurement Unit Block Diagram

A single external resistor, Rg, can be used to set the amplifier gain to any value in the range of 1 to 10000.

$$\text{Amplifier Gain} = [(40{,}000 / RG) + 1] \pm 20\% \qquad (1)$$

A buffer or unity gain amplifier has been added to the system next, followed by a voltage level shifter.

C. Switching System

Switching System design was the most complicated stage in the development process since the electrodes have to be switched automatically in a continuous loop with the constant current injector and the potential measurement units working simultaneously.

Components:

- Analog Multiplexer (CD4051B)
- Microcontroller

Fig. 5 gives the electrode configuration of the proposed system. E1-E8 are the voltage measurement electrodes, and CC is the current injecting electrode pair. CD-4051B is an eight-channel multiplexer and selects one out of the 8 voltage electrode outputs. The control inputs are set by the microcontroller, and the electrodes are switched in a loop accordingly in the set sequence. The complete switching is done using two 4051B ICs. The first IC selects one of the 8 voltage electrode outputs, and the second IC selects the immediate next electrode output. The potential difference is then sent to the Potential Measurement Unit, where the signal is amplified and converted to a digital value using ADC. The process is continuously repeated for all such potential differences.

D. Data Acquisiton System

ADC sampling rate is kept at 1000000 samples per second to remove random noise and stabilize data. Microcontroller based switching is done via 4051B IC and data collected. After the complete measurement is done, data is sent via serial port to a computer for further analysis.

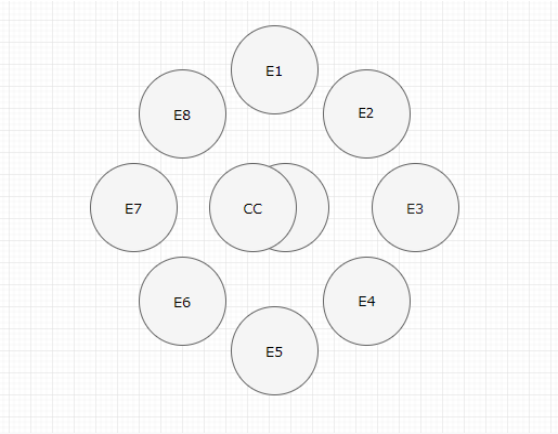

Figure 5. Electrode Configuration

Data acquisition and graph plotting are done using PLX Data Acquisition Tool. This Excel extension receives data directly from a serial port and live plots the resulting graphs in Microsoft Excel. A Phantom model simulating the human chest is designed according to international standards for system testing and performance evaluation. The designed phantom volume was 15 litres. Fig. 6 shows the developed phantom model. All the individual system units are then assembled to complete the proposed system hardware.

III. RESULTS

The performance of the proposed EIT system is evaluated from phantom experimental data. All the individual units are tested first by choosing appropriate tests for each.

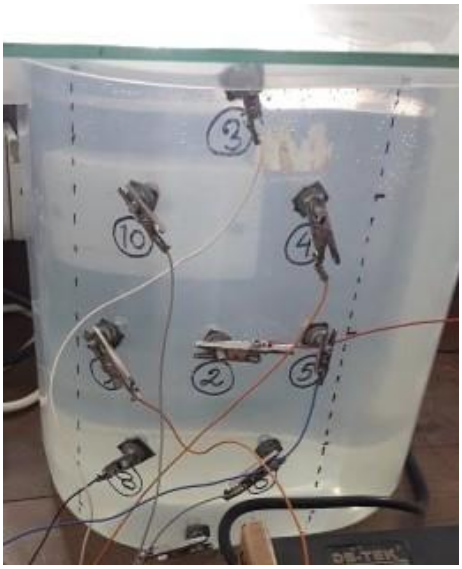

Figure 6. Developed Phantom Model

Performance of the Constant Current Injector**:**
For analyzing the performance of the constant current injector, it is tested for varying loads, and respective output currents are measured. The resulting graph is shown in Fig. 7.

Performance of the Potential Measurement Unit:
The range of our signal of interest is approximately 10mV~100mV, and hence performance is tested by applying input signal within that range. Since the signal amplitude is too small to be accurately measured, the gain is taken to be 27 by setting the gain resistor Rg to 1.5 k Ω. The obtained graph in Fig. 8 shows that for a set gain, input versus output voltage graph is linear, which proves that the gain of the amplifier remains constant over the entire range**.**

Performance of the Switching Module:
The performance of the switching module depends on the switching accuracy and time required for complete switching. The developed switching system is connected to the entire system in multiple stages, which caused a noticeable time delay. But the switching sequence is working perfectly. The system is tested on a phantom, first and complete data acquisition time is around 16 seconds.

A. Phantom Test Cases

The test solution chosen for phantom data acquisition is a salt solution of conductivity 1.52 S/m, which matches the average lung fluid conductivity. The solution was prepared by adding 9 grams of salt per litre of water to fill up the entire phantom volume, and the conductivity was measured using a conductivity meter and set to 1.52 S/m.

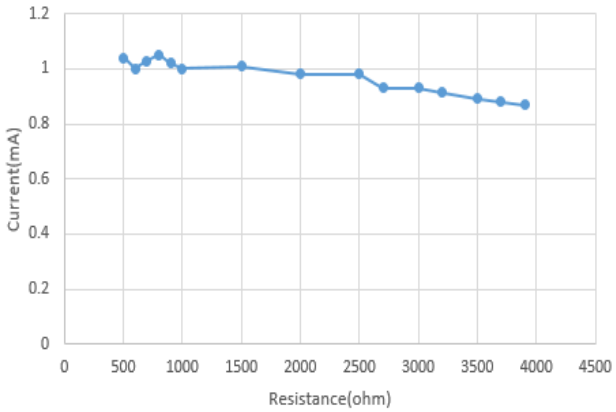

Figure 7. Current Source Load Characteristics

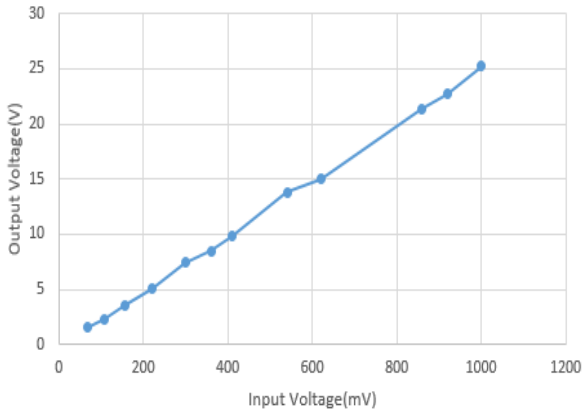

Figure 8. Instrumentation Amplifier Gain Characteristics

Fig. 9 is the graph obtained for uniform conductivity. We have injected a constant sinusoidal current into the phantom. The graph, which is also a sinusoidal waveform, shows correct data collection over cycles in case of homogenous background. The robustness of the proposed system was next evaluated in the presence of anomalies. Most lung diseases change the impedance of a localized area in the lungs, and this is simulated by testing the phantom using anomalies.

a) Testing with Organic Anomaly, Anomaly 1: a potato of volume 230 cubic centimeters

Anomaly 1, which is an organic anomaly, is inserted into the test solution right at the center, and corresponding data collected. Graphs are plotted for 5 complete data cycles. Data collection is done multiple times, and the results are averaged to reduce the effect of noise. The graph in Fig. 10 shows the difference between uniform conductivity and the conductivity when an anomaly is added. Thus the presence of an anomaly can be detected by the system. Introducing Anomaly 1 in the test solution causes a rise in the voltage signal amplitude. Since the current is constant, this means that the resistivity of the solution has also increased. Also, there is a slight phase change indicating a change in the reactance of the solution.

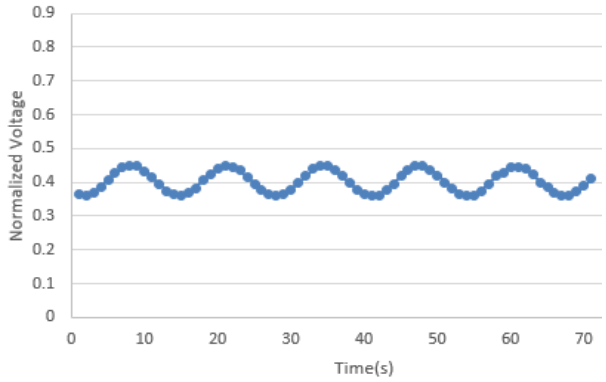

Figure 9. Graph for Salt Solution of Conductivity 1.52 S/m

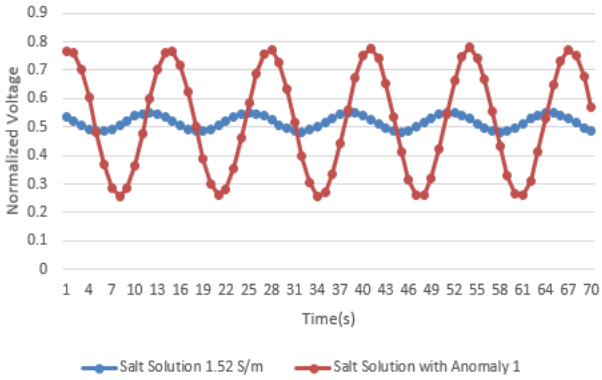

Figure 10. Graph for Anomaly 1 in Salt Solution of Conductivity 1.52 S/m

a) Testing with Inorganic Anomaly, Anomaly 2: a roll of sponge of volume 260 cubic centimeters and density 0.87 grams per cubic centimeter

The next test is carried out using a different type of anomaly. This is done to observe the relationship between the type of anomaly, and the voltage profile obtained. Anomaly 2 is now introduced in the test solution, positioned at the center, and data collected. Multiple data acquisitions are done, and results are averaged to minimize the effect of noise. The graph in Fig. 11 shows the difference between uniform conductivity and conductivity when Anomaly 2 is added. This shows that the addition of this anomaly also leads to an increase in measured voltage amplitude, indicating an increase in resistivity. The difference between the two profiles is due to the nature of the anomalies. For the addition of organic anomalies, there is a large change in conductivity, but the permittivity difference is low. In the case of inorganic anomalies, both conductivity and permittivity changes are significant. The phase shift is thus much more prominent in this case. Since the anomalies were positioned at the center of the phantom, so the phase has changed equally for the entire solution.

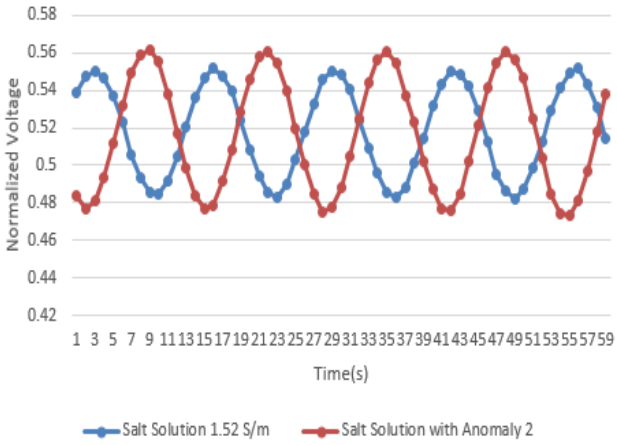

Figure 11. Graph for Anomaly 2 in Salt Solution of Conductivity 1.52 S/m

IV. DISCUSSION

A new EIT system with improved sensitivity, simplicity in design, and less computational complexity has been developed in this research. The proposed EIT system has been implemented in hardware and tested on a human phantom with different anomalies. The change in the impedance profile obtained with the addition of anomalies indicates the ability of the developed system to detect lung diseases. Alam et al. [23, 24] proved that this proposed protocol showed a significant increase in sensitivity in voltage measurement, indicating a change in conductivity of the lungs, compared to various standard protocols for EIT system for lungs. This indicates that the proposed system performs better than other existing protocols. Our obtained waveforms in this paper have closely followed their specific EIT data pattern. Also, obtained voltage amplitude increases, and conductivity falls with the addition of inhomogeneity [12]. In our case, because the inhomogeneities or anomalies were placed at the center of the phantom, amplitude increased equally for the entire solution. Thus the system is working properly and according to theoretical expectations. However, a complete compact system is yet to be developed. Also, the constant current source must be made as accurate as possible. The system was tested using a phantom model. For accurate data acquisition and interpretation, the developed phantom can be modified to represent the human thorax more closely. A replica of the lungs with conductivity matching the human lungs can be placed in the phantom volume to correctly simulate lung conditions. There was an effect of noise in the obtained results, and hence the system noise must be minimized by incorporating appropriate filters and components with better noise stability and also by increasing the repetitions of data acquisitions. The switching system caused the maximum delay in the data collection time, and this delay must be minimized by using faster switching components or alternate algorithms. Images corresponding to the collected data must be generated for easier interpretation of lung diseases. Image reconstruction and analysis need to be incorporated into the system before clinical trials can be carried out.

V. CONCLUSION

Electrical Impedance Tomography (EIT) offers versatile possibilities in medical diagnostic imaging. This work presents a new design of an Electrical Impedance Imaging System, where the current injection electrodes are independent of the measurement set of electrodes, which is different from the existing EIT devices. The system has been successfully developed and tested on phantom lungs for both healthy and diseased conditions, using a homogenous test solution matching the average lung fluid conductivity, as well as different anomalies. The system was working correctly, and the results matched the theoretical interpretations. However, it still needs further improvements and testing in clinical settings before clinical application is possible.

REFERENCES

[1] B. H. Brown, D. C. Barber, and A. D. Seagar, “Applied potential tomography: Possible clinical applications,” *Clin. Phys. Physiol. Meas.*, vol. 6, no. 2, pp. 109–121, 1985.

[2] I. Frerichs, “Electrical impedance tomography (EIT) in applications related to lung and ventilation: A review of experimental and clinical activities,” *Physiol. Meas.*, vol. 21, no. 2, 2000.

[3] A. Adler and A. Boyle, “Electrical impedance tomography: Tissue properties to image measures,” *IEEE Trans. Biomed. Eng.*, vol. 64, no. 11, pp. 2494–2504, 2017.

[4] G. Hahn *et al.*, “Imaging pathologic pulmonary air and fluid accumulation by functional and absolute EIT,” *Physiol. Meas.*, vol. 27, no. 5, 2006.

[5] M. Assenheimer *et al.*, “The T-SCAN TM technology : electrical impedance as a diagnostic tool for breast cancer detection,” *Physiol. Meas.*, vol. 1, pp. 1–8, 2001.

[6] S. Krueger-Ziolek *et al.*, “Multi-layer ventilation inhomogeneity in cystic fibrosis,” *Respir. Physiol. Neurobiol.*, vol. 233, pp. 25–32, 2016.

[7] A. Borsic, R. Halter, Y. Wan, A. Hartov, and K. D. Paulsen, “Sensitivity study and optimization of a 3D electric impedance tomography prostate probe,” *Physiol. Meas.*, vol. 30, no. 6, 2009.

[8] M. Bodenstein, M. David, and K. Markstaller, “Principles of electrical impedance tomography and its clinical application,” *Crit. Care Med.*, vol. 37, no. 2, pp. 713–724, 2009.

[9] S. BARIŠIN, “Electrical impedance tomography as ventilation monitoring in ICU patients,” *Signa vitae J. intesive care Emerg. Med.*, vol. Volume 14, no. Supplement 1, pp. 21–23, 2018.

[10] I. Frerichs *et al.*, “High-frequency oscillatory ventilation in patients with acute exacerbation of chronic obstructive pulmonary disease,” *J. Crit. Care*, vol. 27, no. 2, pp. 172–181, 2012.

[11] L. T. Muftuler, M. Hamamura, O. Birgul, and O. Nalcioglu, “Resolution and contrast in magnetic resonance electrical impedance tomography (MREIT) and its application to cancer imaging,” *Technol. Cancer Res. Treat.*, vol. 3, no. 6, pp. 599–609, 2004.

[12] G. Singh, S. Anand, B. Lall, A. Srivastava, V. Singh, and H. Singh, “Practical phantom study of low cost portable EIT based cancer screening device,” *2016 IEEE Long Isl. Syst. Appl. Technol. Conf. LISAT*, pp. 1-6, 2016.

[13] K. Y. Aristovich, G. S. Dos Santos, B. C. Packham, and D. S. Holder, “A method for reconstructing tomographic images of evoked neural activity with electrical impedance tomography using intracranial planar arrays,” *Physiol. Meas.*, vol. 35, no. 6, pp. 1095–1109, 2014.

[14] T. de C. Martins *et al.*, “A review of electrical impedance tomography in lung applications: Theory and algorithms for absolute images,” *Annu. Rev. Control*, vol. 48, pp. 442–471, 2019.

[15] V. Tomicic and R. Cornejo, “Lung monitoring with electrical impedance tomography: Technical considerations and clinical applications,” *J. Thorac. Dis.*, vol. 11, no. 7, pp. 3122–3135, 2019.

[16] L. Yang, S. Yue, Z. Wang, X. Liu, and H. Wang, “3D printed chest models with realistic shape and electrical property for electrical impedance tomography,” *I2MTC 2019 - 2019 IEEE Int. Instrum. Meas. Technol. Conf. Proc.*, vol. 2019-May, no. 61573251, pp. 1–5, 2019.

[17] B. Gong, S. Krueger-Ziolek, K. Moeller, B. Schullcke, and Z. Zhao, “Electrical impedance tomography: Functional lung imaging on its way to clinical practice?,” *Expert Rev. Respir. Med.*, vol. 9, no. 6, pp. 721–737, 2015.

[18] I. Frerichs, Z. Zhao, T. Becher, P. Zabel, N. Weiler, and B. Vogt, “Regional lung function determined by electrical impedance tomography during bronchodilator reversibility testing in patients with asthma,” *Physiol. Meas.*, vol. 37, no. 6, pp. 698–712, 2016.

[19] L. F. Fuks, M. Cheney, D. Isaacson, D. G. Gisser, and J. C. Newell, “Detection and Imaging of Electric Conductivity and Permittivity at Low Frequency,” *IEEE Trans. Biomed. Eng.*, vol. 38, no. 11, pp. 1106–1110, 1991.

[20] G. Hahn, I. Sipinkova, F. Baisch, and G. Hellige, “Changes in the thoracic impedance distribution under different ventilatory

conditions," *Physiol. Meas.*, vol. 16, no. 3A, 1995.

[21] W. Durlak and P. Kwinta, "Role of Electrical Impedance Tomography in Clinical Practice in Pediatric Respiratory Medicine," *ISRN Pediatr.*, vol. 2013, pp. 1–5, 2013.

[22] T. K. Bera, "Applications of Electrical Impedance Tomography (EIT): A Short Review," *IOP Conf. Ser. Mater. Sci. Eng.*, vol. 331, no. 1, pp. 22–25, 2018.

[23] Alam, M.S., Md. Adnan Kiber, and S.M. Mostafa Al Mamun, "Simulation study of electrical impedance changes of normal lung compared to diseased lung of pulmonary edema using comsol multiphysics software," *International Conference on Physics in Medicine & Clinical Neuroelectrophysiology*, pg-53, 2017.

[24] Alam, M.S., S.M. Mostafa Al Mamun, and Md. Adnan Kiber, "Improved Electrical Impedance Measurement (EIM) Method for Lung Disease Detection," *International Conference on Physics in Medicine (IPCM)*, pg-64, 2020.